Deuterium permeation through multi-layer ceramic coatings under liquid lithium-lead exposure condition

Deuterium permeation through multi-layer ceramic coatings under liquid lithium-lead exposure condition

Erika Akahoshi[a], Moeki Matsunaga[a], Keisuke Kimura[a], Kazuki Nakamura[a], Kazuki Saito[b], Yoshimitsu Hishinuma[b,c], Teruya Tanaka[c], Takumi Chikada[a*]

[a]Shizuoka University, 836 Ohya, Suruga-ku, Shizuoka 422-8529, Japan

[b]The Graduate University for Advanced Studies, SOKENDAI, 322-6 Oroshi, Toki, Gifu 509-5292, Japan

[c]National Institute for Fusion Science, 322-6 Oroshi, Toki, Gifu 509-5292, Japan

*Corresponding author's email: chikada.takumi@shizuoka.ac.jp

Abstract

Corrosion of tritium permeation barrier ceramic coatings by liquid tritium breeders is an unavoidable concern in a high thermal efficiency fusion reactor. In this study, we have established a deuterium permeation measurement system under static Li-Pb exposure conditions to investigate the deuterium permeation behavior of multi-layer ceramic coatings under corrosive environments. The system successfully detected the coating degradation on the moment by measuring an irregular increase in deuterium permeation. The permeation behaviors showed that the coating degraded more seriously as the number of the interfaces between the different ceramics increased.

Keywords: A. Ceramic; B. SEM; C. Hydrogen permeation; C. Oxide coatings; C. Interfaces

1. Introduction

Tritium permeation through structural materials is a critical issue in fusion reactor blanket systems from the viewpoints of fuel loss and radiological safety. One of the promising technical solutions to the problem is to install a tritium permeation barrier (TPB) on the components such as blanket chassis and metal pipes. Ceramic coatings have been investigated as TPBs using various coating materials and methods and showed sufficient permeation reduction [1–3]. Metal organic decomposition (MOD) is a liquid-phase coating method that is promising due to its capability to fabricate on the components with complicated geometries. Another unavoidable concern in high thermal efficiency liquid blanket concepts is corrosion of the TPB coating by liquid tritium breeders such as lithium-lead (Li-Pb) alloy. In our previous studies, hydrogen isotope permeation reduction performance and the static Li-Pb compatibility of single-layer coatings prepared by MOD have been separately investigated [4–6]. More recently, an Er_2O_3-ZrO_2 two-layer coating showed higher permeation reduction performance than the single-layer coatings [7]. Moreover, the Li-Pb corrosion resistance of the multi-layer coating was improved by increasing the number of the coating fabrication process, although some layer structures showed degradation after Li-Pb exposure [8]. In the context of the previous works, multi-layer coatings have the potential for the simultaneous pursuit of hydrogen isotope permeation reduction and Li-Pb corrosion resistance. Toward the application to an actual reactor, it is necessary for the coating to maintain the permeation reduction performance under high-temperature environments with tritium breeders. The hydrogen isotope permeation experiments with Li-Pb exposure were carried out using a few TPB coatings [9–11]. These papers were sporadically reported, and the experiments were conducted using unique systems. That is why the precise permeation mechanism in the coating and the relationship between the permeation and Li-Pb corrosion have yet to be revealed. Therefore, in this study, the deuterium permeation measurement system under static Li-Pb exposure has been established to investigate the permeation behavior of the coatings under

liquid Li-Pb blanket environments. Besides, the timing of coating degradation was considered by monitoring the deuterium permeation flux continuously, which was impossible in static Li-Pb exposure experiments.

2. Experimental details

2.1. Sample preparation

Squared plates of reduced activation ferritic/martensitic steel F82H (Fe-8Cr-2W, F82H-BA07 heat) with dimensions of 25 mm in length and 0.5 mm in thickness were used as substrates. The coating procedure is described in detail in Refs. [6,7]. The substrates for multi-layer coating samples were heat-treated before the MOD process to form a chromium oxide (Cr_2O_3) thin layer that plays a role to prevent peeling of the MOD coating due to the formation of iron oxide on the substrate during multiple heat treatments [12]. The heat-treatment was conducted for 10 min at 710 ºC in high purity argon and hydrogen mixture flow with a volume ratio of 1:1 by setting each flow rate as 50 standard cubic centimeters per minute (sccm). Thereafter, the Cr_2O_3-formed substrates were dipped into the metal-organic liquids (Er-03® for Er_2O_3 and SYM-ZR-04® for ZrO_2, Kojundo Chemical Laboratory Co., Ltd.) and pulling up with a constant speed of 1.0 mm s^{-1} using a dip coater. Just after pulling up, the samples were dried at 150 ºC for 6 min and pre-heated at 550 ºC for 2 min in air on hot plates. The processes of dipping, drying, and pre-heating were repeated three times for single-layer coating and twice for multi-layer coatings. After that, the samples were heat-treated at 700 ºC for 30 min in argon and hydrogen mixture flow with each flow rate of 50 sccm to crystallize the coatings without the formation of the iron oxide from the substrate. To fabricate multi-layer coatings, the series of the processes including the heat treatment were repeated four times. The layer compositions of the coatings are summarized in Fig. 1. The thicknesses of the ZrO_2 single-layer coating and the multi-layer coatings were approximately 200 nm and 400–450 nm, respectively, which was confirmed by

cross-sectional observation. The heat treatments for the Er_2O_3-ZrO_2 two-layer coating and the Er_2O_3-ZrO_2-Er_2O_3-ZrO_2 four-layer coating were conducted the same number of times to unify the stress during coating fabrication.

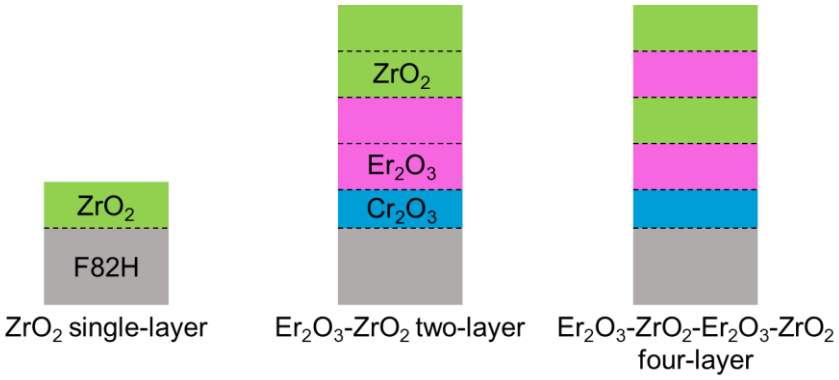

Fig. 1. Layer structures of coating samples.

2.2. Deuterium permeation test under static Li-Pb exposure

The sketch of the apparatus for the deuterium permeation test under static Li-Pb exposure is shown in Fig. 2. This was assembled based on the gas-driven permeation measurement system described in Ref. [13]. A sample is sealed with two stainless C-rings with an Inconel coil spring inside (U-TIGHTSEAL®, Usui Co, Ltd.). In this study, the coated side was set upward facing the upstream. Li-Pb was synthesized from 99.9 % Li and 99.999 % Pb ingots purchased from Furuuchi Chemical Co. with an atomic ratio of 15.7:84.3 under argon atmosphere in a glove box. Li-Pb of approximately 1.3 cm^3 was poured into the upstream pipe of 12.7 mm in outer diameter and 1 mm in wall thickness, then the height of Li-Pb was approximately 1.4 cm with consistently covering the surface of the sample. In this system, the coated side of the sample was exposed to static Li-Pb.

The procedure of the permeation test was followed by Ref. [13]. The ion current of deuterium permeated through Li-Pb and the sample was measured using a quadrupole mass spectrometer (QMS)

and converted to the deuterium permeation flux with a calibration factor obtained using a deuterium standard leak. A thermocouple was placed in the sample part in contact with the backside of the sample. The test temperature was set at 300–600 ºC, and the tests were conducted from lower temperatures. The driving pressure of deuterium to the upstream was set to 10.0–80.0 kPa. If the permeation is limited by atomic diffusion in a sample, the deuterium permeation flux per permeation area J (mol m^{-2} s^{-1}) through a sample with a thickness d (m) is expressed by the following equation [14]:

$$J = P\frac{p^{0.5}}{d} \quad (1)$$

where P (mol m^{-1} s^{-1}) is the permeability and p (Pa) is the driving pressure. If the rate-determining process of permeation is molecular processes such as surface reactions, the linear relationship between J and p is expected. In this study, the permeation fluxes were compared at the driving pressure of 80.0 kPa, which is the highest pressure and then has the smallest effect on surface reactions. It should be noted that we assumed the deuterium permeability in Li-Pb had a linear dependence with temperature in this study [15], which allowed us to extrapolate the permeation data at lower temperatures to higher temperatures.

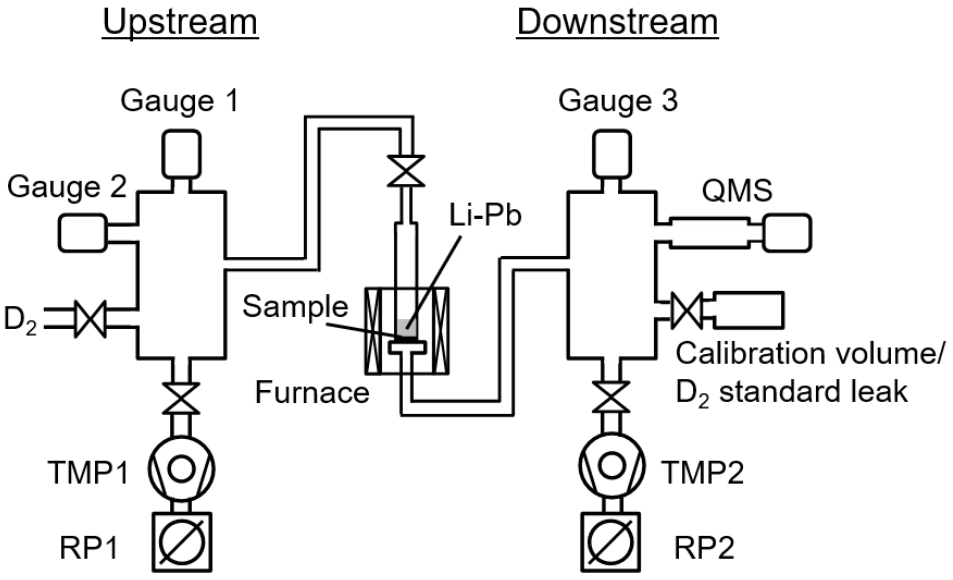

Fig. 2. Schematic view of the apparatus for deuterium permeation test under static Li-Pb exposure.

2.3. Microstructure analysis

After the deuterium permeation test under static Li-Pb exposure, Li-Pb was melted by a heating container and removed from the sample assembly. Then, the sample was picked up from the assembly and shook out the adhered Li-Pb. No cleaning process using ethanol and acetic acid was done to avoid potential damage to the coating. Surface and cross-sectional observations for the samples were conducted by field emission scanning electron microscopy (FE-SEM) with energy dispersive X-ray spectroscopy (EDX) located at National Institute for Fusion Science, Japan and Forschungszentrum Jülich, Germany. Cross-sectional SEM observation and EDX analysis of selected areas were performed using a focused ion beam system or a cross section polisher. Crystallographic information of the sample was obtained by X-ray diffraction (XRD).

3. Results and discussion

3.1. F82H substrate

Fig. 3 shows the driving pressure dependence of the deuterium permeation flux for the uncoated F82H substrate with Li-Pb. The pressure exponent estimated by curve fitting was 0.77 and 0.73 at 350 and 400 °C, respectively. In the deuterium permeation tests using the uncoated F82H substrate without Li-Pb, the exponent value was around 0.5, which indicates the rate-determining process of the deuterium permeation through the sample was atomic diffusion [16]. These results suggest that the permeation through Li-Pb was limited by a hybrid regime that atomic diffusion and surface reactions are equally contributed. The existence of Li-Pb or the change of the Li-Pb free surface would be the cause of the difference in the exponent value between the permeation tests for the F82H

substrates with and without Li-Pb. Fig. 4 shows temperature dependence of deuterium permeation flux for the uncoated F82H substrate with Li-Pb. The permeation flux of the F82H substrate with Li-Pb was an order of magnitude lower than that of the F82H substrate without Li-Pb [16]. Hereafter, the results of the permeation tests under static Li-Pb exposure using coating samples are discussed in comparison with that using the F82H substrate with Li-Pb.

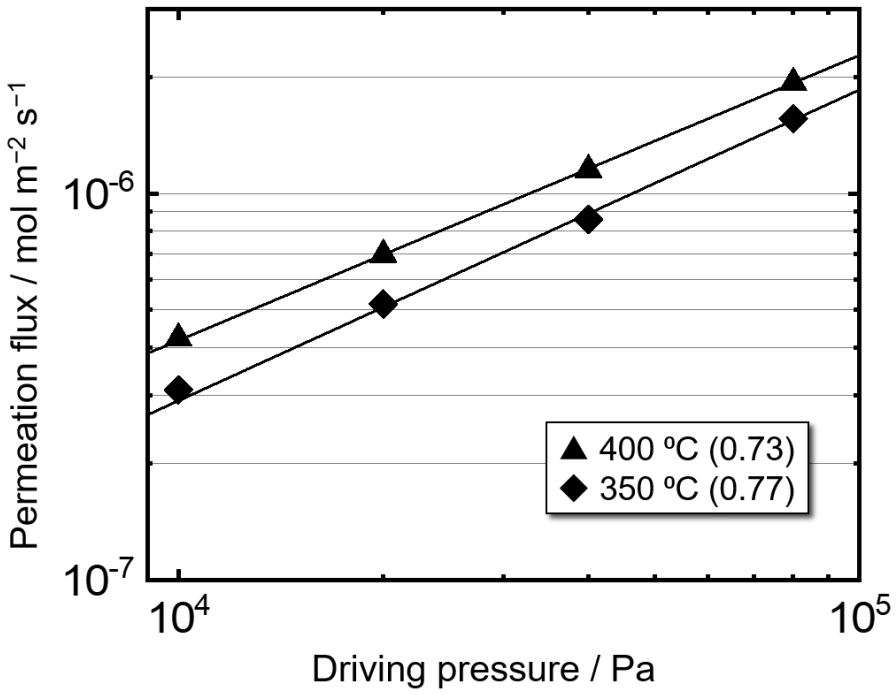

Fig. 3. Driving pressure dependence of deuterium permeation flux for uncoated F82H substrate with Li-Pb. Numbers in parenthesis represent the pressure exponent *n*.

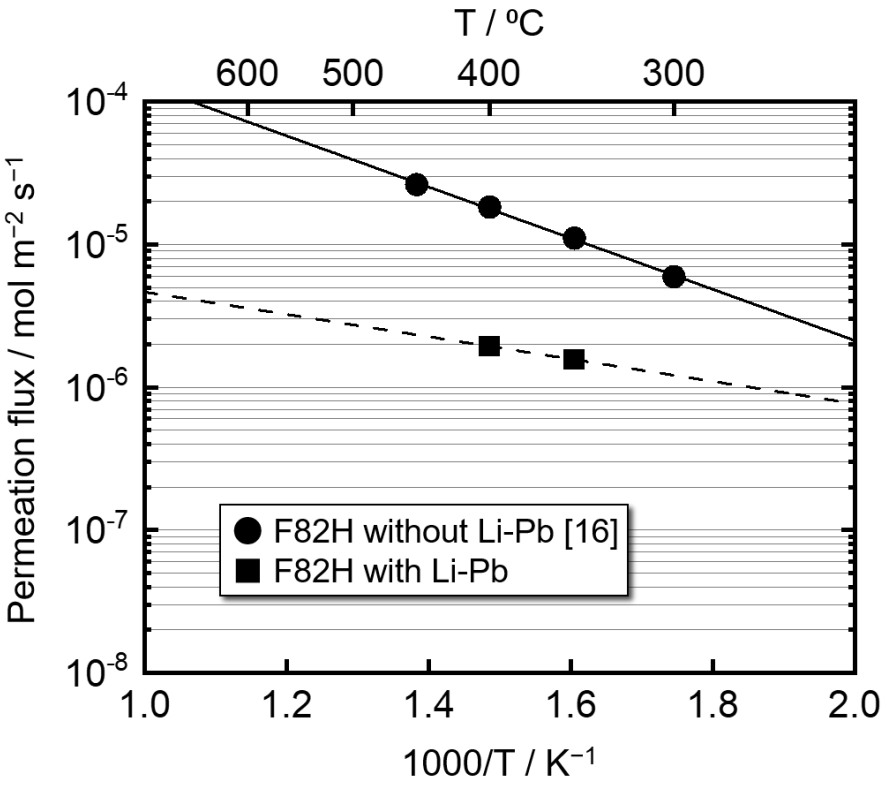

Fig. 4. Arrhenius plots of deuterium permeation flux for uncoated F82H substrate with Li-Pb. Reference data of F82H without Li-Pb is also presented [16].

3.2. ZrO_2 single-layer coating

Fig. 5 shows the results of the deuterium permeation tests under static Li-Pb exposure for the ZrO_2 single-layer coating. The deuterium permeation flux decreased by two orders of magnitude in comparison with that of the F82H substrate at 500 °C due to crystallization and/or grain growth of the coating. After that, the permeation flux did not increase significantly even at 600 °C; therefore, no degradation might occur in the coating. On the other hand, an increase in the permeation flux due to coating degradation was observed in the permeation test at 600 °C without Li-Pb [5]. A possible reason why the coating did not degrade during the permeation measurement at 600 °C would be that Li-Pb might prevent impurities from reaching the coating and suppress the degradation. In particular, moisture is an unavoidable impurity gas desorbed from the steel surface in the vacuum system.

Oxygen dissociated from moisture would diffuse in the coating followed by oxidation of the substrate, resulting in a decrease in coating adhesion [17]. Although the driving pressure dependence of the permeation flux as shown in Fig. 3 was not presented for the coated samples, the pressure exponent was around 0.5 for all the coated samples in the following sections. That indicates the permeation through the coating after crystallization and/or grain growth was limited by atomic diffusion in the coating. Also, it is proved the permeation flux through the coating is much lower than the uncoated F82H substrate with Li-Pb in which the permeation is fast enough.

The surface and cross-sectional SEM images of the ZrO_2 coating before and after the permeation tests are shown in Fig. 6. No significant change in surface structure, such as crack formation and delamination of the coating, was observed after the permeation tests. From the SEM observation, the coating did not degrade up to 600 °C with Li-Pb. White particles seen at the interface between the ZrO_2 layer and the substrate in Fig. 6(d) would be Pb transported from above during the cross-sectional processing. The thickness of the ZrO_2 layer increased after the tests: from approximately 200 nm to 300 nm, possibly due to the expansion with the formation of a corrosion product.

Fig. 7 shows the XRD spectra of the sample before and after the permeation tests. Lithium zirconate (Li_2ZrO_3) was detected after the tests, indicating that the ZrO_2 coating reacted with Li-Pb and Li_2ZrO_3 formed as a corrosion product. ZrO_2 would be corroded by the following reaction between Li and dissolved O in Li-Pb, as suggested in our previous study [8]:

$$ZrO_2 + 2Li + O[Li] \rightarrow Li_2ZrO_3 \quad (2)$$

Another point worth mentioning is that the tetragonal phase of ZrO_2 mostly changed to the monoclinic phase after the tests. The phase change was accompanied by an approximately 4 % volume expansion, which might be a cause of coating degradation. In this case, the coating did not degrade during the tests probably because the density of the coating before the tests would be lower than the ideal value, and there was sufficient space for expansion during the phase change. The peak sharpness also indicates that the grain size of the coating is smaller than bulk polycrystalline ceramics. Moreover,

179 the phase change might contribute to the decrease in the permeation flux at 500 °C. It should be noted
180 that the spectrum after the permeation tests included the outside of the permeated area where the
181 coating was exposed to the air at high temperatures. That is the reason why the spectrum showed the
182 peaks derived from Cr_2O_3 and Fe.

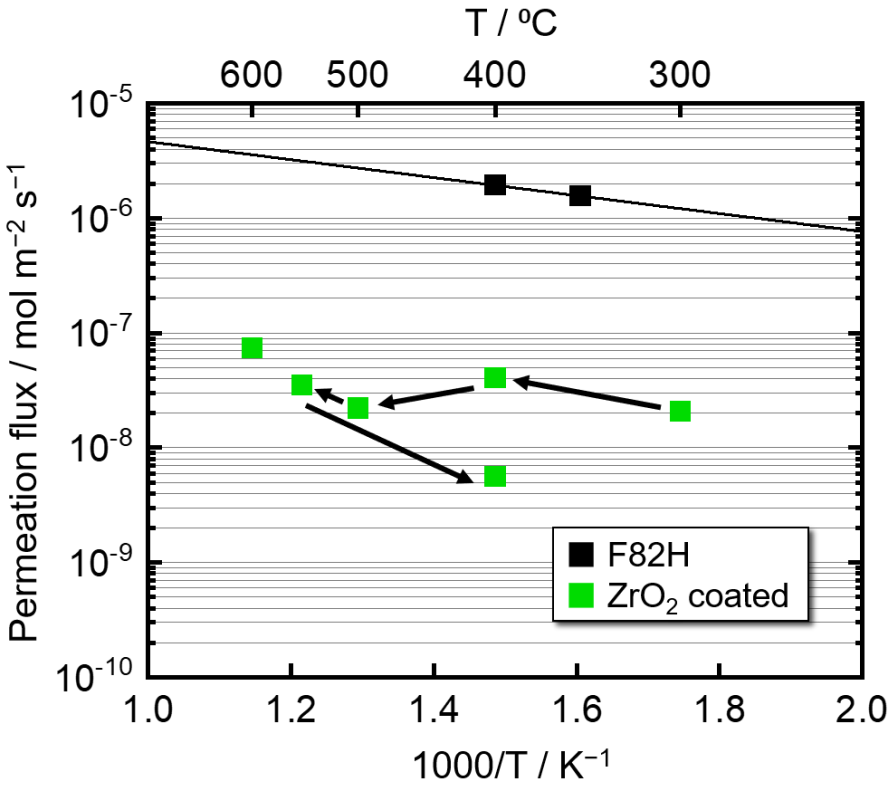

183

184 Fig. 5. Arrhenius plots of deuterium permeation flux under static Li-Pb exposure for uncoated
185 F82H substrate and the ZrO_2 single-layer coating sample.

186

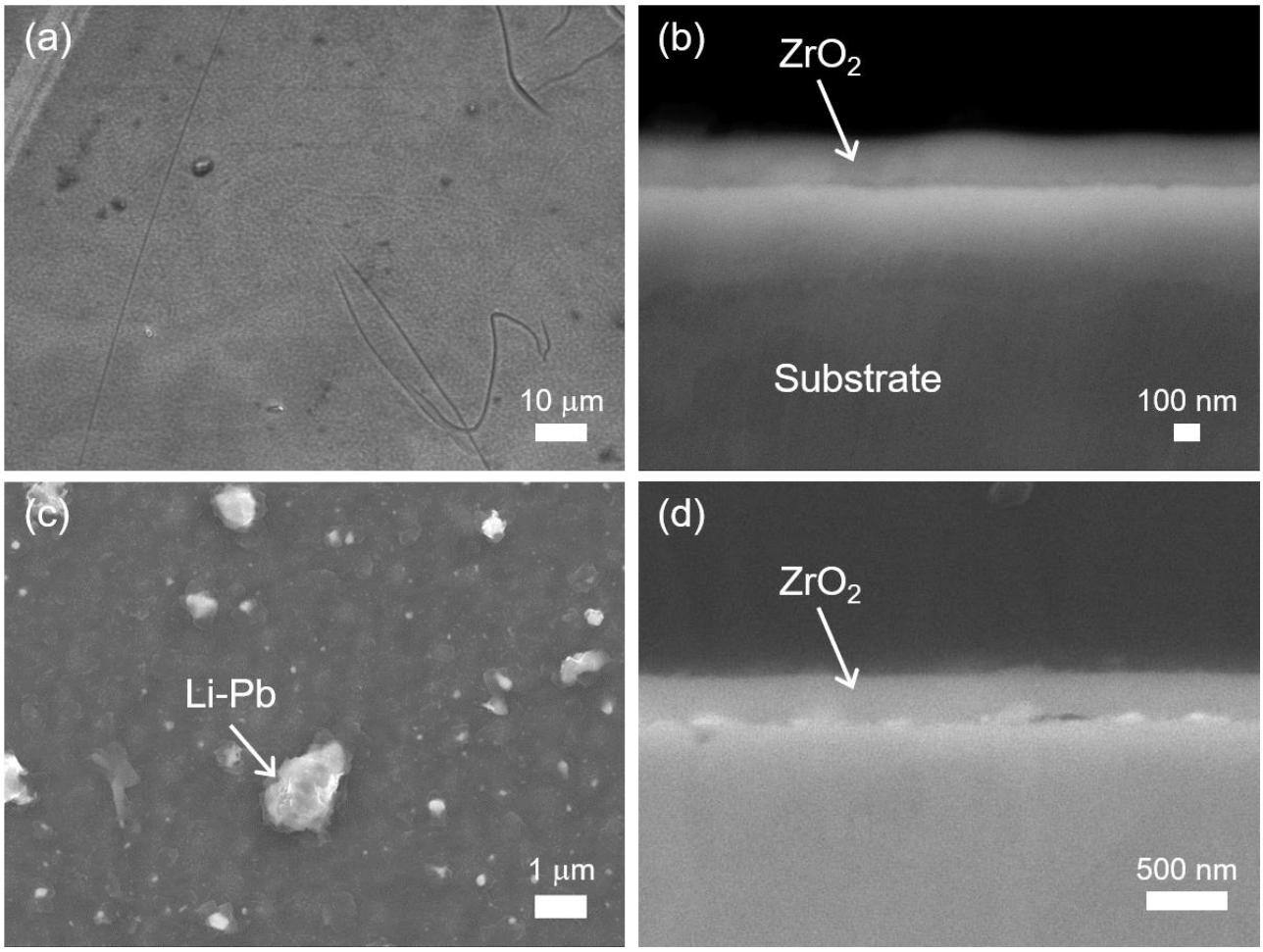

Fig. 6. Surface and cross-sectional SEM images of the ZrO_2 single-layer coating sample (a,b) before and (c,d) after the permeation tests under static Li-Pb exposure.

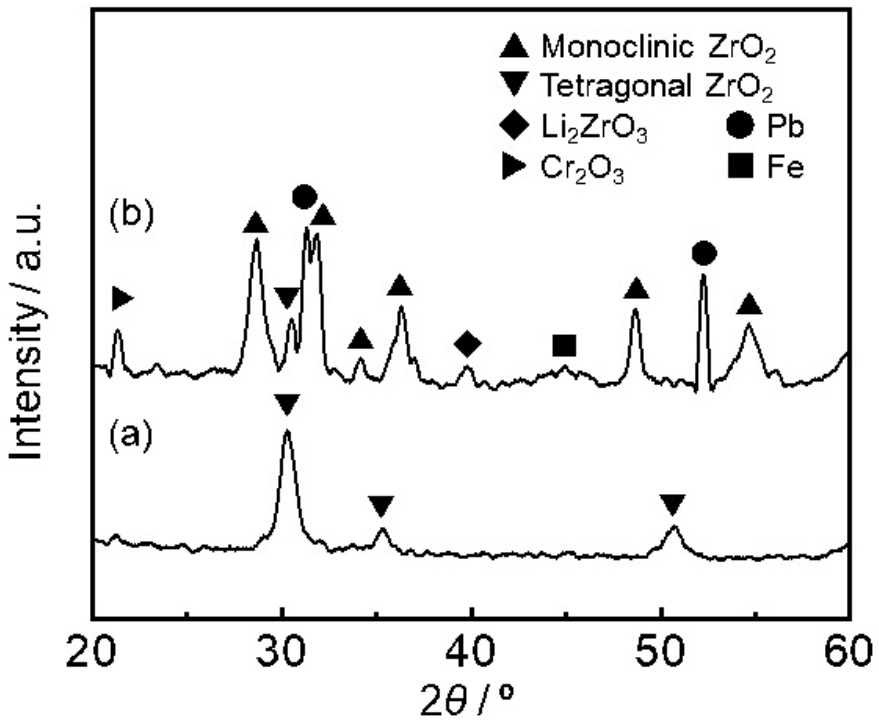

Fig. 7. XRD spectra of ZrO_2 single-layer coating sample (a) before and (b) after the permeation tests under static Li-Pb exposure.

3.3. Er_2O_3-ZrO_2 two-layer coating

Fig. 8 shows the results of the permeation tests for the Er_2O_3-ZrO_2 two-layer coating. The deuterium permeation flux decreased by a factor of 100 in comparison with that of the F82H substrate at 400 °C due to crystallization and/or grain growth. The temperature when the permeation flux started decreasing was different between the single-layer and two-layer coating samples might relate to the difference of the number of the heat-treatment for the ZrO_2 layer. After the permeation flux decreasing at 400 °C, the permeation flux changed as temperature increased up to 550 °C but significantly increased at 600 °C. Therefore, the degradation might occur in the coating during the test temperature changing from 550 °C to 600 °C. In the following test at 400 °C, however, the permeation flux was three orders of magnitude lower than that of the F82H substrate and one order of magnitude lower

than that in the first test.

Fig. 9 shows the surface and cross-sectional SEM images of Er_2O_3-ZrO_2 coating sample before and after the permeation tests. Cracks were observed after the tests, which might contribute to the unexpected increase in the permeation flux at 600 °C. Generally speaking, the cracking is caused by the internal stress in the coating. The internal stress is created by the difference in the coefficient of thermal expansion (CTE) among the coatings and substrate. The CTE of Er_2O_3, ZrO_2, Cr_2O_3, and the F82H substrate at room temperature are approximately 6×10^{-6}, 8×10^{-6}, 10×10^{-6}, and 11×10^{-6} K^{-1}[18–20], respectively. When the temperature changed during the test, the stress created by the CTE mismatch is applied to the coatings and the cracking would occur at a certain stage to release the stress. However, even with the cracks formed in the coating, the permeation flux did not increase to the level of the substrate in the test at 600 °C. Moreover, the lower permeation flux was confirmed in the second 400 °C test compared to that in the first test. From these results, we consider that the corrosion product such as Li_2ZrO_3 was produced during the tests and inhibited the permeation. In particular, in the test at 400 °C, the deposition of the corrosion product on the coating and/or the blocking of the gaps due to the substrate shrinkage would result in a drastic decrease in the permeation flux. In the cross-sectional micrograph after the tests (Fig. 9(d)), no cracks were observed, which suggests the cracks shown in Fig. 9(c) were locally generated. The thickness of the ZrO_2 layer increased from approximately 300 nm to 500 nm, indicating the formation of the corrosion product, as also shown in the ZrO_2 single-layer coating in the previous section

In our previous study using the Er_2O_3-ZrO_2 two-layer coating, no cracks were observed after the static Li-Pb exposure tests for up to 2000 h at 600 °C [12]. One of the large differences between the static Li-Pb exposure test and the permeation test under static Li-Pb exposure was the sample placement method. During the permeation test under static Li-Pb exposure, the sample was tightened up using metal sealings. In this case, the mechanical stress should be concentrated on the coating, leading to coating degradation. That also indicates that the mechanical strength of the coatings

degraded by Li-Pb exposure. The evaluation of mechanical properties before and after microstructural change and Li-Pb exposure would be necessary for a precise prediction of the lifetime of the coatings in an actual reactor.

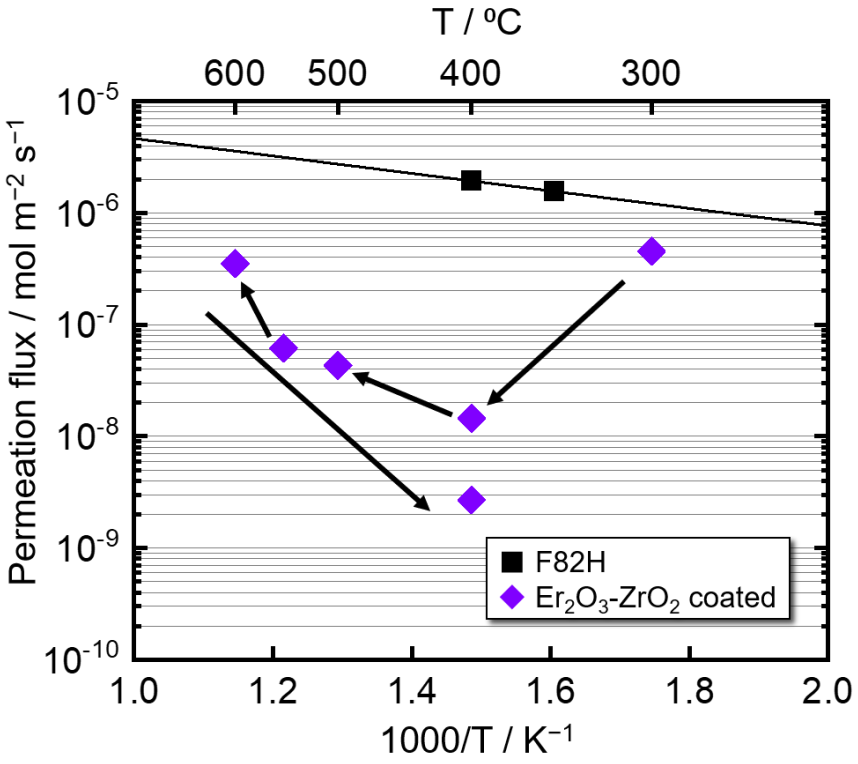

Fig. 8. Arrhenius plots of deuterium permeation flux under static Li-Pb exposure for uncoated F82H substrate and the Er_2O_3-ZrO_2 two-layer coating sample.

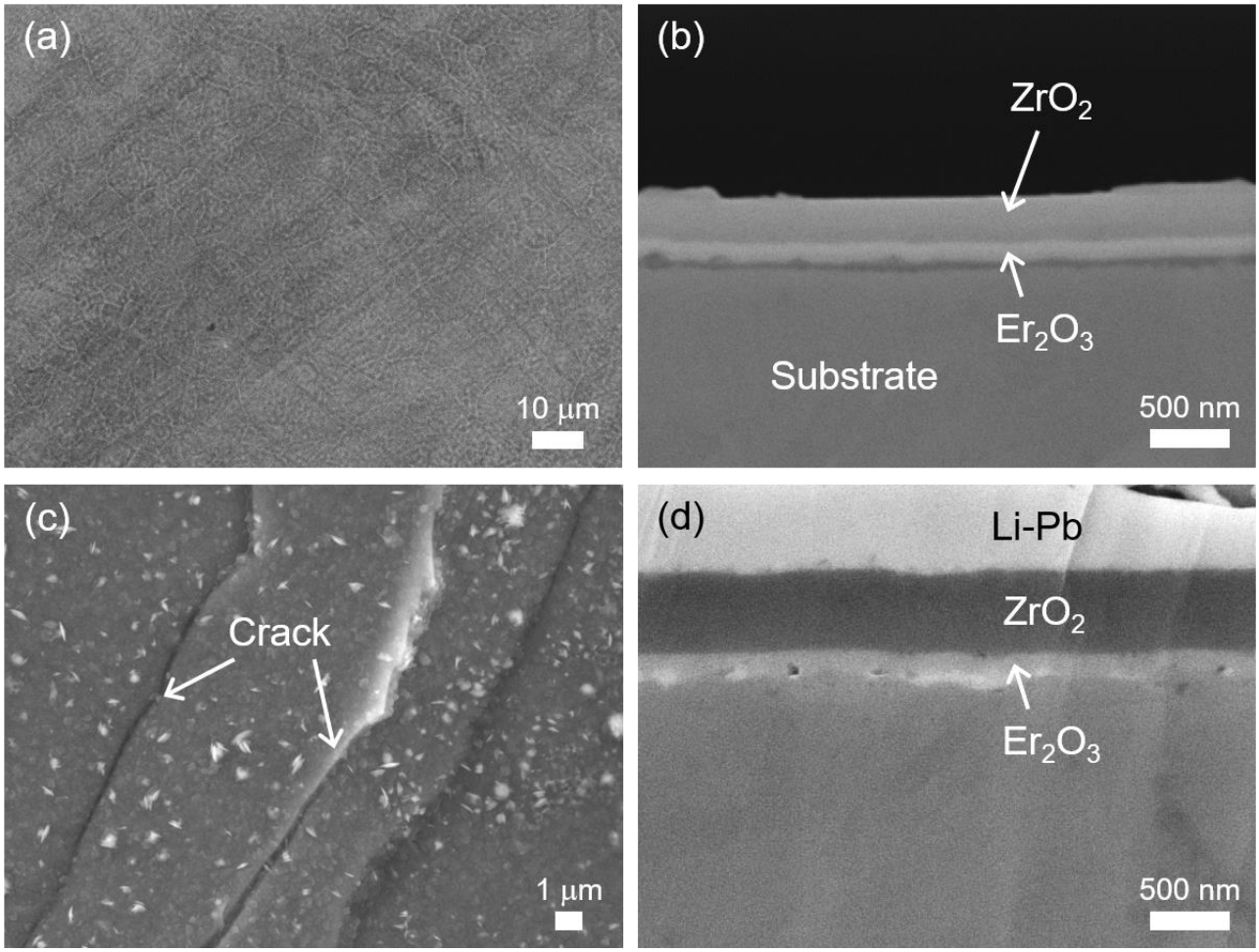

Fig. 9. Surface and cross-sectional SEM images of the Er_2O_3-ZrO_2 two-layer coating sample (a,b) before and (c,d) after the permeation tests under static Li-Pb exposure.

3.4. Er_2O_3-ZrO_2-Er_2O_3-ZrO_2 four-layer coating

Fig. 10 shows the results of the permeation tests for the Er_2O_3-ZrO_2-Er_2O_3-ZrO_2 four-layer coating sample. The crystallization and/or grain growth occurred at 400–600 °C, and the permeation flux decreased by a factor of 800 in comparison with that of the F82H substrate at 600 °C. However, a precipitous increase in the permeation flux was observed during the test at 600 °C. The temporal change of the permeation flux in the test at 600 °C is shown in Fig. 11. At the beginning of the test, the permeation flux decreased with decreasing the driving pressure of deuterium introduced to the

upstream; however, the drastic and irregular increase in the permeation flux was observed when the driving pressure was kept at 20.0 kPa. This trend is typical in the test when the coating forms cracks and peelings; therefore, the in-situ detection of the coating degradation during the test at 600 °C was achieved. The discontinuous increase in the permeation flux is considered to be caused by the cracking in several steps. In the second test at 400 °C, the permeation flux decreased by four orders of magnitude in comparison with that of the F82H substrate, which is the trend similar to the result of the Er_2O_3-ZrO_2 two-layer coating, as shown in Fig. 8. The difference in the permeation behavior of the four-layer coating from the single-layer and the two-layer coatings would be attributed to the four-layer structure which needed higher temperatures to promote crystallization and/or grain growth. After the irregular increase in the permeation flux during the test at 600 °C, 10 thermal cycles were applied to the sample by cooling down to less than 100 °C in an hour and heating up to 600 °C in an hour with a driving deuterium pressure of 80.0 kPa. The permeability at 600 °C decreased to 55 % after 10 thermal cycles, which suggests no further coating degradation was proceeded under the thermal cycles.

Fig. 12 shows the surface and cross-sectional SEM images of the Er_2O_3-ZrO_2-Er_2O_3-ZrO_2 four-layer coating sample before and after the permeation tests. After the permeation tests, the peelings were observed over the large region. From cross-sectional SEM image, in addition, the loss of the four-layer coatings was confirmed in the peeled region. Despite the large peeling, the permeation flux was two orders of magnitude lower than that of the substrate at 600 °C. The surface coverage of the coating after degradation was estimated using the permeation data before degradation and the equation described in detail in Ref. [21]. Fig. 13 shows the calculated permeation flux of the Er_2O_3-ZrO_2-Er_2O_3-ZrO_2 four-layer coating sample at 600 °C as a function of surface coverage with the deuterium permeation flux of uncoated F82H and the coating sample before degradation. From the measured permeation flux after degradation at 600 °C, the estimated surface coverage of the coating was 0.99. The contradiction between the experimental results and the calculation indicates another

274 factor. As explained in the previous section, it is highly possible that the permeation flux would be
275 inhibited by the corrosion product and blocking of the gaps due to the substrate shrinkage in the
276 second test at 400 °C. The two-digit difference between the permeation flux at 400 °C and 600 °C
277 also suggests that the solubility of the corrosion product in Li-Pb may change depending on
278 temperature.

279 The Er_2O_3-ZrO_2-Er_2O_3-ZrO_2 four-layer coating has interfaces between the different ceramic
280 materials; therefore, the larger stress from the CTE mismatch might be applied to the interfaces than
281 the Er_2O_3-ZrO_2 two-layer coating and cause the cracking over the large region. The coating might be
282 easily peeled when the sample was picked up from the test apparatus after the permeation tests. The
283 exposure of the substrate surface due to peeling indicates that the more extensive cracking might
284 occur in the Er_2O_3-ZrO_2-Er_2O_3-ZrO_2 four-layer coating in comparison with the Er_2O_3-ZrO_2 two-layer
285 coating. From these results, the timing of the coating degradation should not be after the tests but
286 during the Li-Pb exposure at high temperatures (≥ 600 °C). Besides, as the number of the interfaces
287 between the different ceramics increased, the coating degradation was more seriously after the
288 permeation tests under static Li-Pb exposure. This result is common to the results of the static Li-Pb
289 exposure test [8], but more sensitively expressed in the measurement system applying the mechanical
290 stress.
291

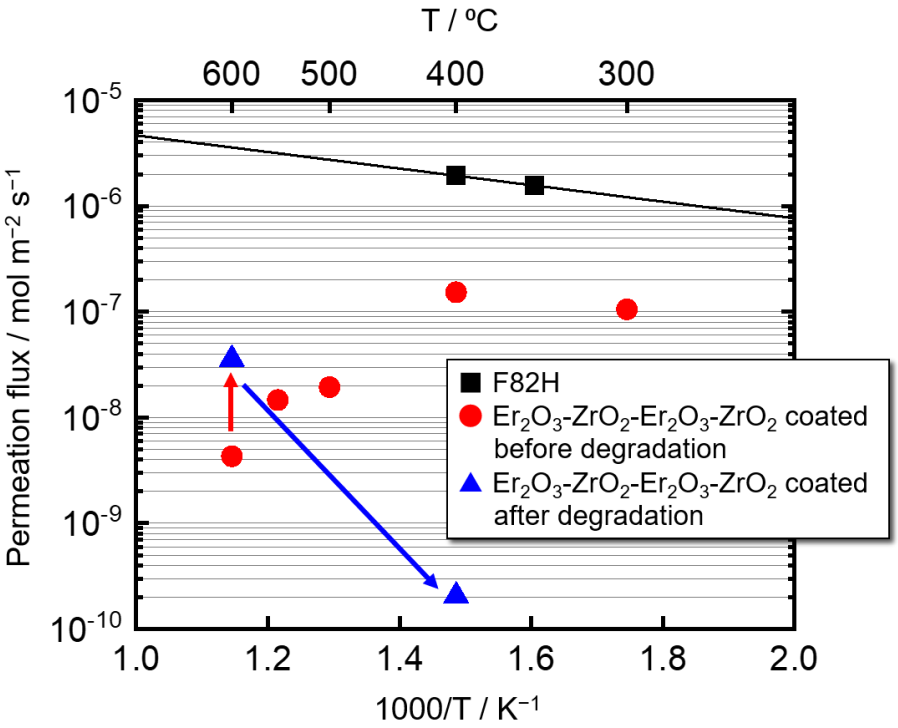

Fig. 10. Arrhenius plots of deuterium permeation flux under static Li-Pb exposure for uncoated F82H substrate and Er_2O_3-ZrO_2-Er_2O_3-ZrO_2 four-layer coating sample.

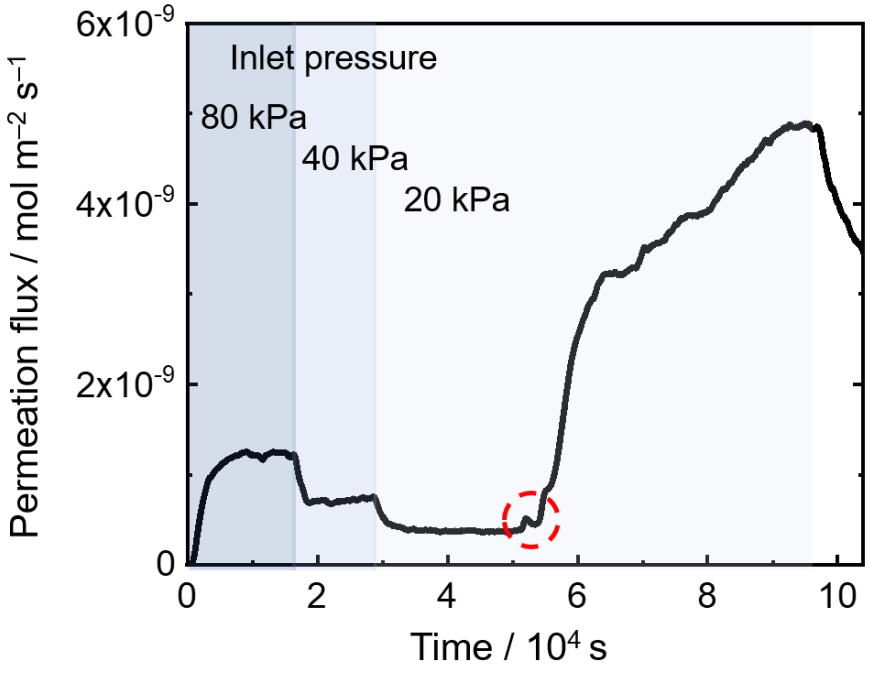

Fig. 11. Temporal change of deuterium permeation flux in the permeation test under static Li-Pb

exposure at 600 ºC for the Er_2O_3-ZrO_2-Er_2O_3-ZrO_2 four-layer coating sample.

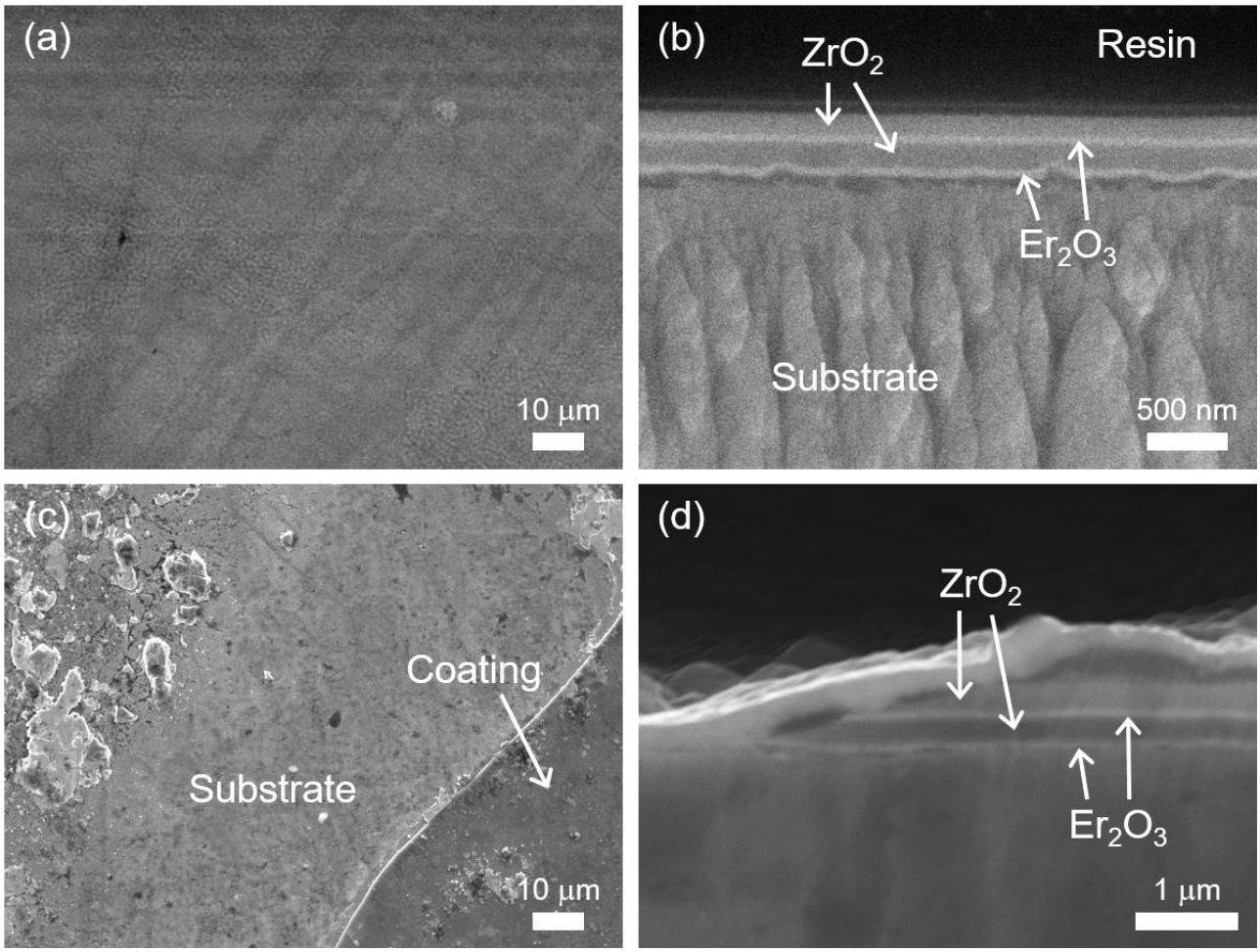

Fig. 12. Surface and cross-sectional SEM images of Er_2O_3-ZrO_2-Er_2O_3-ZrO_2 four-layer coating sample (a,b) before and (c,d) after the permeation tests under static Li-Pb exposure.

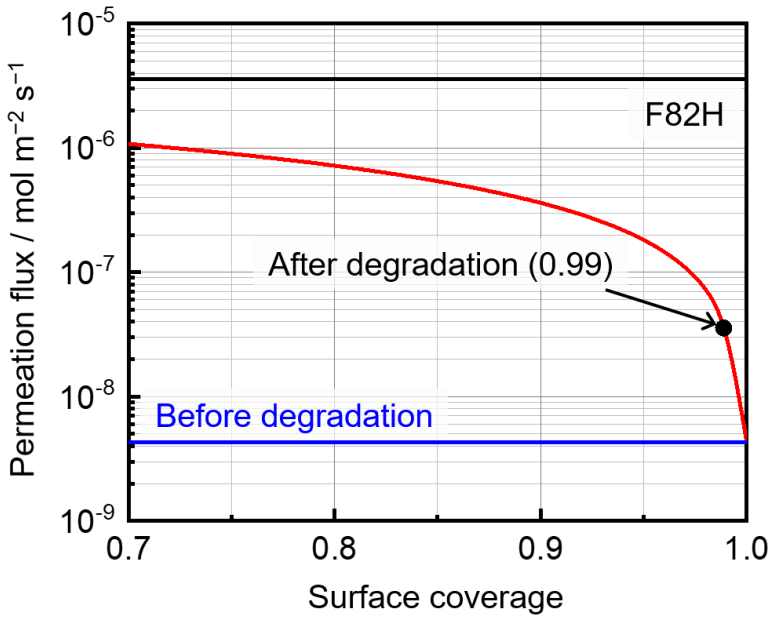

Fig. 13. Calculated sample surface coverage at 600 ºC with permeation flux of uncoated F82H substrate and Er_2O_3-ZrO_2-Er_2O_3-ZrO_2 four-layer coating sample. The horizontal lines representing the flux of F82H substrate and four-layer coating sample before degradation were obtained from experimental results.

4. Conclusion

Deuterium permeation measurements under static Li-Pb exposure were conducted to investigate the permeation reduction performance of the single and multi-layer coatings under a Li-Pb corrosion environment. Also, the temporal changes in the permeation flux were observed to clarify the timing of the coating degradation. In the permeation tests using the ZrO_2 single-layer coating sample, the coating did not degrade, and the permeation reduction performance of the coating was maintained throughout the tests. The permeation flux increased during the permeation tests using the Er_2O_3-ZrO_2 two-layer coating sample, and the cracks were observed after the tests. The permeation flux discontinuously increased during the permeation test using the Er_2O_3-ZrO_2-Er_2O_3-ZrO_2 four-layer coating sample. Since the widespread peelings and exposure of the substrate were observed after the

tests, the in-situ detection of the coating degradation was achieved using the permeation system. The suppression of the permeation probably due to the corrosion product was confirmed after the degradation of the two-layer and four-layer coatings, resulting in three and four orders of magnitude lower permeation fluxes than the uncoated substrate. It is found that the timing of the coating degradation is during the Li-Pb exposure at high temperatures. Moreover, the coating degraded more seriously after the permeation test under static Li-Pb exposure as the number of the different ceramic interfaces increased. The number of the interfaces between the different ceramics should be reduced to maintain the permeation reduction performance of the coatings.

Acknowledgements

This work was supported by JSPS KAKENHI Grant Number 19H01873 and the NIFS Collaboration Research program (NIFS18KEMF119).

References

[1] G.W. Hollenberg et al., Tritium/hydrogen barrier development, Fusion Eng. Des. 28 (1995) 190–208.

[2] J. Konys et al., Status of Tritium Permeation Barrier Development in the EU, Fusion Sci. Technol. 47 (2005) 844–850.

[3] T. Chikada, Ceramic Coatings for Fusion Reactors, in: R. Konings and R. Stoller (Eds.), Comprehensive Nuclear Materials 2nd edition, Elsevier, Oxford, 2020, pp. 274–283.

[4] T. Chikada et al., Deuterium permeation through erbium oxide coatings on RAFM steels by dip-coating technique, J. Nucl. Mater. 442 (2013) 533–537.

[5] T. Chikada et al., Fabrication technology development and characterization of tritium permeation barriers by a liquid phase method, Fusion Eng. Des. 136 (2018) 215–218.

[6] M. Matsunaga et al., Lithium-lead corrosion behaviors of erbium oxide, yttrium oxide and

zirconium oxide coatings prepared by metal organic decomposition, J. Nucl. Mater. 511 (2018) 534–543.

[7] J. Mochizuki et al., Preparation and characterization of Er_2O_3-ZrO_2 multi-layer coating for tritium permeation barrier by metal organic decomposition, Fusion Eng. Des. 136 (2018) 219–222.

[8] E. Akahoshi et al., Corrosion tests of multi-layer ceramic coatings in liquid lithium-lead, Fusion Eng. Des. 160 (2020) 111874.

[9] T. Terai et al., Tritium permeation through austenitic stainless steel with chemically densified coating as a tritium permeation barrier, Fusion Eng. Des. 212–215 (1994) 976–980.

[10] A. Aiello et al., Qualification of tritium permeation barriers in liquid Pb-17Li, Fusion Eng. Des. 69 (2003) 245–252.

[11] M. Nakamichi et al., In-pile tritium permeation through F82H steel with and without a ceramic coating of Cr_2O_3–SiO_2 including $CrPO_4$, Fusion Eng. Des. 82 (2007) 2246–2251.

[12] T. Tanaka et al., Control of substrate oxidation in MOD ceramic coating on low-activation ferritic steel with reduced-pressure atmosphere, J. Nucl. Mater. 45 (2014) 630–634.

[13] T. Chikada et al., Deuterium permeation behavior of erbium oxide coating on austenitic, ferritic and ferritic/martensitic steels, Fusion Eng. Des. 84 (2009) 590–592.

[14] E. Serra et al., Influence of traps on the deuterium behavior in the low activation martensitic steels F82H and Batman, J. Nucl. Mater. 245 (1997) 108–114.

[15] S. Fukada et al., Clarification of Tritium Behavior in Pb-Li Blanket System, Mater. Trans. 54 (2013) 425–429.

[16] T. Chikada etal., Surface behavior in deuterium permeation through erbium oxide coatings, Nucl. Fusion 51 (2011) 063023.

[17] T. Chikada et al., Compatibility of tritium permeation barrier coatings with ceramic breeder pebbles, Corros. Sci. 182 (2021) 109288.

[18] S. Singh et al., Thermal expansion of erbium, thulium, and ytterbium sesquioxides, J. Amer.

370 Ceram. Soc. (1970) 53 (3) 169.
371 [19] H. Scheibe, Ceramic canning materials for nuclear fuels, Interceram. (1965) 1 34–34, 43–44.
372 [20] A.-A.F. Tavassoli et al., Materials design data for reduced activation martensitic steel type F82H,
373 Fusion Eng. Des. 61–62 (2002) 617–628.
374 [21] T. Chikada et al., Modeling of tritium permeation through erbium oxide coatings, Fusion Sci.
375 Technol. 60 (2011) 389–393.